Tidal dynamics in the Gulf of Maine and New England Shelf: An application of FVCOM

Changsheng Chen,[1,2] Haosheng Huang,[3] Robert C. Beardsley,[4] Qichun Xu,[1] Richard Limeburner,[4] Geoffrey W. Cowles,[1] Yunfang Sun,[1] Jianhua Qi,[1] and Huichan Lin[1]

Received 14 February 2011; revised 19 September 2011; accepted 29 September 2011; published 10 December 2011.

[1] The unstructured-grid, Finite-Volume Community Ocean Model (FVCOM) was used to simulate the tides in the Gulf of Maine (GoM) and New England Shelf (NES) for homogeneous and summer stratified conditions. FVCOM captures the near-resonant nature of the semidiurnal tide and energy flux in the GoM and the complex dynamics governing the tide in the NES. Stratification has limited impact on tidal elevation, but can significantly modify the tidal current profile. Internal tides are energetic in the stratified regions over steep bottom topography, but their contribution to the total tidal energy flux is only significant over the northeast flank of Georges Bank. The model suggests that the tidal flushing-induced eddy east of Monomoy Island is the dynamic basis for the locally observed phase lead of the M_2 tide. The southward propagating tidal wave east of Cape Cod encounters the northeastward propagating tidal wave from the NES south of Nantucket Island, forming a zone of minimum sea level along a southeast-oriented line from Nantucket Island. These two waves are characterized by linear dynamics in which bottom friction and advection are negligible in the momentum balance, but their superposition leads to a strong nonlinear current interaction and large bottom stress in the zone of lowest sea elevation.

Citation: Chen, C., H. Huang, R. C. Beardsley, Q. Xu, R. Limeburner, G. W. Cowles, Y. Sun, J. Qi, and H. Lin (2011), Tidal dynamics in the Gulf of Maine and New England Shelf: An application of FVCOM, *J. Geophys. Res.*, *116*, C12010, doi:10.1029/2011JC007054.

1. Introduction

[2] Tidal dynamics in the Gulf of Maine (GoM) and New England Shelf (NES) region have been the focus of much study over the last 40 years (Figure 1). The GoM region is characterized by large semidiurnal M_2 (12.42 h) tidal currents with the world's highest tidal range of over 8 m occurring in the upper reaches of the Bay of Fundy (BF) [*Garrett*, 1972]. The lowest natural surface gravity wave mode in the GoM/BF system has a period of ~12.8 h and a harmonic oscillator quality factor $Q \sim 3$, resulting in an enhanced tidal response over the entire semidiurnal frequency band due to the near-resonant geometry of the GoM/BF system [*Garrett*, 1974; *Greenberg*, 1979]. In addition to the shallow BF and adjoining shoal area south of Cape Sable, Nova Scotia, semidiurnal currents are strong over the two shallow submarine banks – Georges and Browns Banks – that separate the deeper inner GoM from the North Atlantic [*Bigelow*, 1927]. Over the southern flank of Georges Bank (GB), the M_2 tide is dynamically akin to a Sverdrup wave propagating across the Bank [*Brown*, 1984]. In contrast, the Mid-Atlantic Bight and Scotian Shelf have resonant frequencies far above the semidiurnal band [*Clarke*, 1991] and the semidiurnal currents are weaker. Tidal currents in Nantucket Sound, Nantucket Shoals and the adjacent shelf region in the NES feature complex spatial variability [*Haight*, 1942; *Beardsley et al.*, 1977; *Shearman and Lentz*, 2004], due in part to the complex bathymetry in this transition zone between the Mid-Atlantic Bight and GoM/BF tidal regimes.

[3] Tides in the GoM/GB region have been investigated using both finite difference [*Greenberg*, 1979, 1983; *Chen et al.*, 2001] and finite element [*Lynch and Naimie*, 1993] numerical circulation models. All of these studies reproduced the general observed features of the M_2 tide. For example, *Lynch and Naimie* [1993] used the 3-D unstructured-grid finite element model QUODDY and reported that the model-data differences (standard deviations) are 2.3 cm in amplitude and 3° in phase over 49 stations for elevation, and are 6.6 cm/s in major axis, 5.4 cm/s in minor axis, 13° in phase and 13° in orientation over 72 stations for currents. Similar results were reported by *Chen et al.* [2001], who used the modified Princeton Ocean Model (ECOM-si) but focused

[1]School for Marine Science and Technology, University of Massachusetts Dartmouth, New Bedford, Massachusetts, USA.
[2]Also at Marine Ecosystem and Environment Laboratory, College of Marine Science, Shanghai Ocean University, Shanghai, China.
[3]Department of Oceanography and Coastal Sciences, School of the Coast and Environment, Louisiana State University, Baton Rouge, Louisiana, USA.
[4]Department of Physical Oceanography, Woods Hole Oceanographic Institution, Woods Hole, Massachusetts, USA.

0148-0227/11/2011JC007054

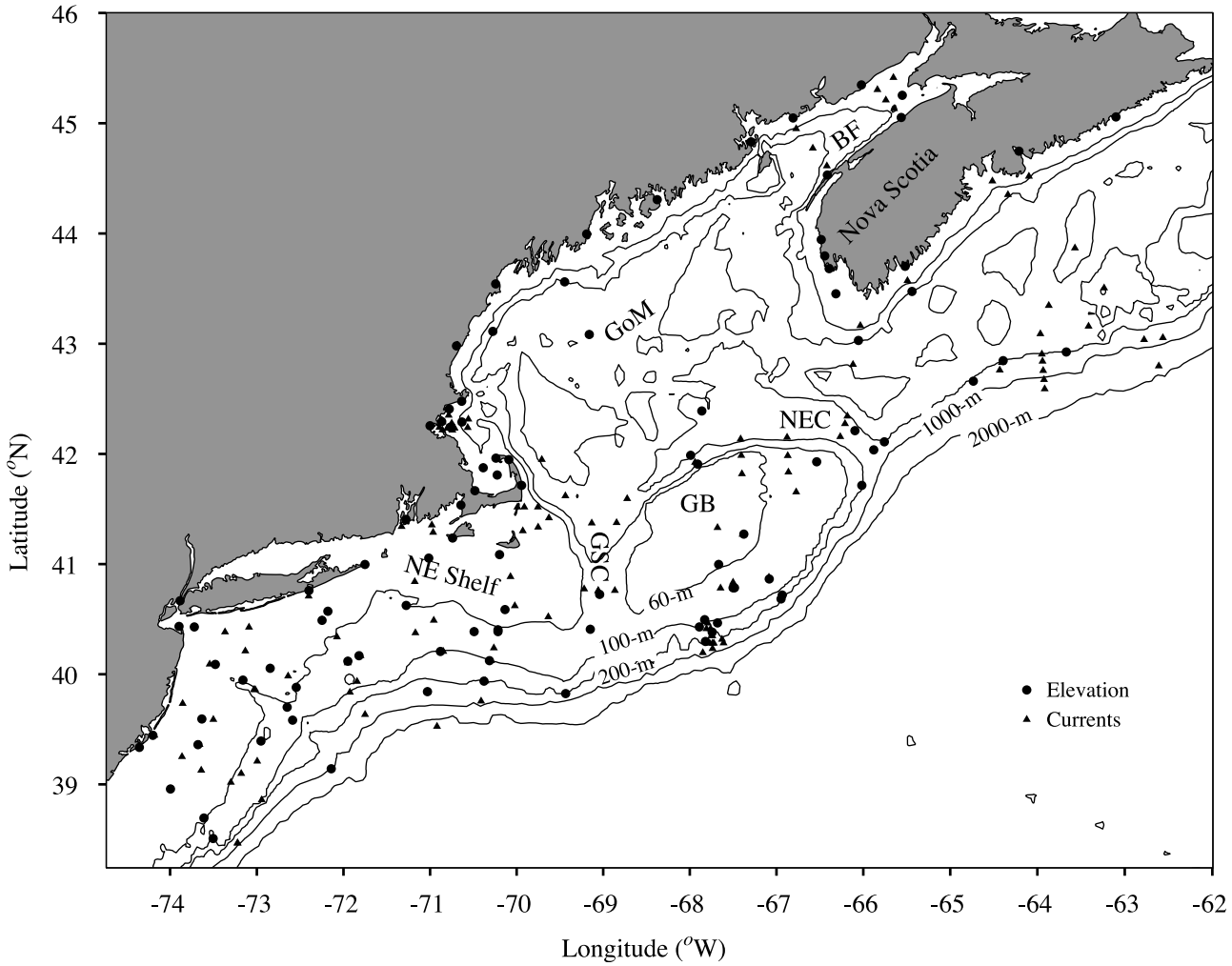

Figure 1. Bathymetry of the southern New England continental margin including the New England Shelf (NES), the Gulf of Maine (GoM), Georges Bank (GB), Great South Channel (GSC), Bay of Fundy (BF), the Northeast Channel (NEC), and the Scotian shelf off Nova Scotia. Filled triangle and filled dot symbols denote the sites of current and surface elevation measurements used in the model-data comparisons.

their model-data comparison on stations in the western GoM/GB.

[4] We have developed an unstructured-grid Finite-Volume Community Ocean Model (FVCOM) [*Chen et al.*, 2003, 2006a, 2006b, 2007]. This model features a non-overlapping unstructured triangular grid in the horizontal and a generalized terrain-following coordinate in the vertical, and solves the integral form of the governing equations by second-order accurate flux-based finite-volume methods. FVCOM thus takes advantage of the geometric flexibility of finite element methods and computational efficiency of finite difference methods. The flux calculation approach ensures mass conservation in individual computational volumes, with no numerical smoothing needed to preserve numerical stability.

[5] In this paper, we use FVCOM to simulate the eight dominant tidal constituents in the GoM/GB/NES region. In addition to validating this model through comparison to observational data and previous model results, we examine the impacts of water stratification on tidal dynamics in the GoM/GB region and tidal-driven processes over the NES. The energy budgets for barotropic and baroclinic tides are estimated to quantify the contribution of internal tides.

[6] This paper is organized as follows. In section 2, FVCOM and the design of the numerical experiments are described. In section 3, the model-data comparisons for tidal elevation and currents are summarized and the roles of stratification and internal tides are discussed. In section 4, the M_2 tide and currents in the Nantucket Sound/Shoals area are presented, followed by a discussion of the governing dynamics. In section 5, the conclusions are summarized.

2. FVCOM and Design of Numerical Experiments

[7] Numerical experiments in this study are made using FVCOM [*Chen et al.*, 2003, 2006a, 2006b] with a default setup of the modified Mellor and Yamada level 2.5 (MY-2.5) and Smagorinsky turbulent closure schemes for vertical and horizontal mixing, respectively [*Mellor and Yamada*, 1982; *Smagorinsky*, 1963]. The governing equations in

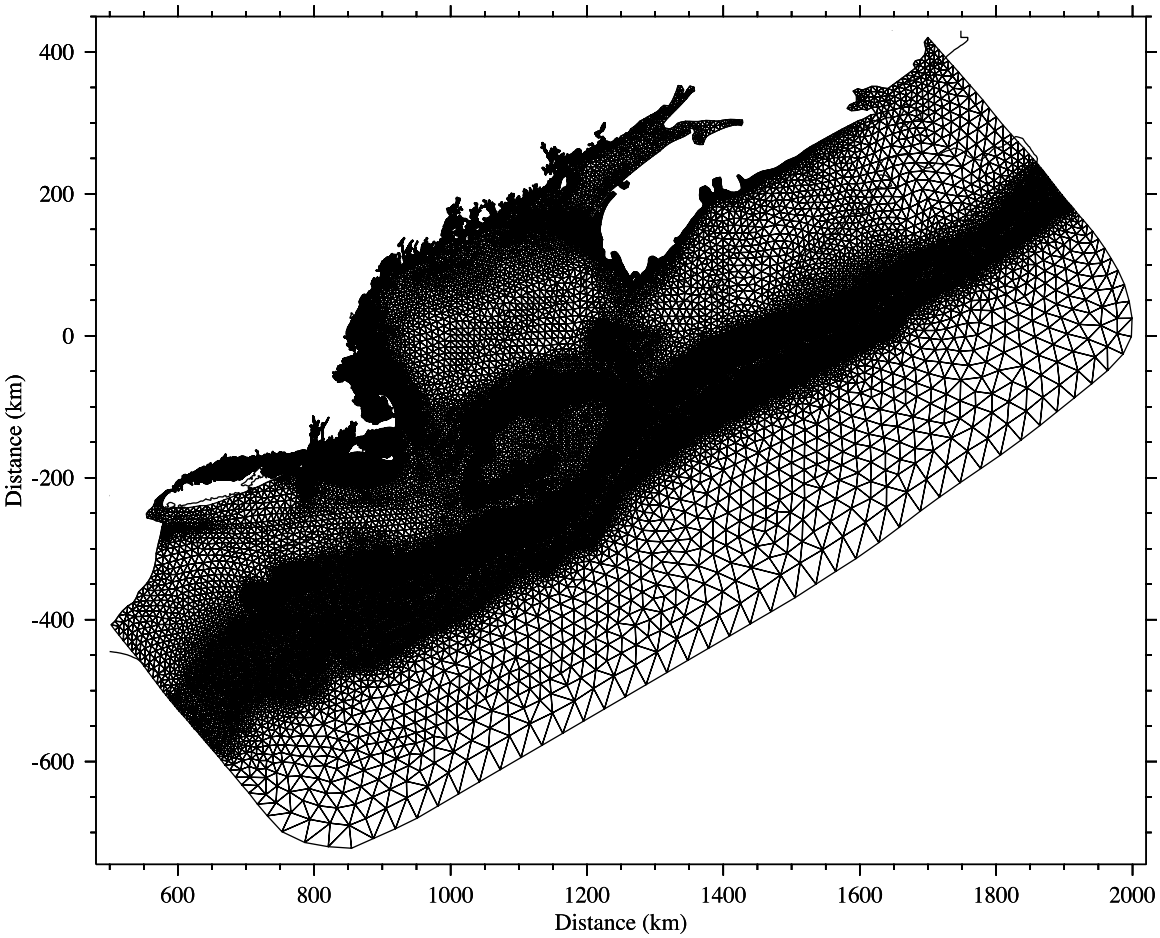

Figure 2. Unstructured triangular grid of FVCOM for the GoM/GB/NES regional tidal model used in this study. Horizontal resolution (ΔL) is measured using the length of the longest sideline of a triangular cell. ΔL varies from 0.3 km-1.0 km near the coast and on GB to 15 km near the open boundary.

FVCOM are discretized by an integral form over control volumes in which the advection terms are solved by a second-order accuracy upwind finite-volume flux scheme [*Kobayashi et al*., 1999; *Hubbard*, 1999] integrated in time using the modified explicit fourth-order Runge–Kutta (RK4) time stepping scheme. The vertical diffusion terms in FVCOM are calculated using a fully implicit finite-volume flux scheme. In this study, FVCOM is integrated using a mode-split solver in which external and internal modes are advanced in tandem at different time steps.

[8] The numerical domain of FVCOM covers the GoM/GB/NES region and is enclosed by an open boundary running from the New Jersey shelf to the Nova Scotia shelf (Figure 2). The horizontal grid has a resolution (measured by the length of the longest edge of a triangular cell) that varies from 0.5 km to 10 km over the entire domain. Over GB, the resolution is 0.5–1.0 km over the steep northern flank, 2.0–3.0 km over the crest, and 1.0–2.0 km around the shelf break region of the southern flank. The resolution in the BF ranges from 0.5 km inside inlets to 2.0 km along the coast and 4.0 km in the interior of the Bay. Over the NES, the resolution is 0.3–0.5 km. The vertical grid discretization is implemented using a hybrid terrain-following coordinate with a total of 45 layers [*Chen et al.*, 2009]. In regions with depth greater than 225 m, 10 and 5 uniform layers with a thickness of 5 m are used near the surface and bottom respectively. In regions of depth less than 225 m, a sigma distribution with a uniform layer thickness is used. The coordinate transition thus occurs smoothly at a depth of 225 m where all layers have a uniform thickness of 5 m. This hybrid coordinate allows us to better resolve the surface mixed layer and bottom boundary layer dynamics over sloping topography while maintaining the vertical resolution in the shallow shelf and coastal regions. The mean water depths at all nodes were determined using the most current version of the high-resolution USGS 15-arcsec digital bathymetry data set [*Roworth and Signell*, 1998], with a minimum depth of 3 m applied at the coast.

[9] FVCOM is forced by a prescribed surface elevation at the open boundary. This forcing is the sum of periodic functions specified by the amplitudes and phases of the eight major tidal constituents [M_2 (12.42 h), N_2 (12.66 h), S_2 (12.00 h), K_2 (11.97 h), K_1 (23.93 h), O_1 (25.82 h), P_1(24.07 h) and Q_1(26.87 h)], which have been obtained through interpolation from the *Egbert and Erofeeva* [2002] 1/6° inverse tidal model results. No open boundary condition is required for currents in FVCOM, since they are located at the center of each triangular cell and are

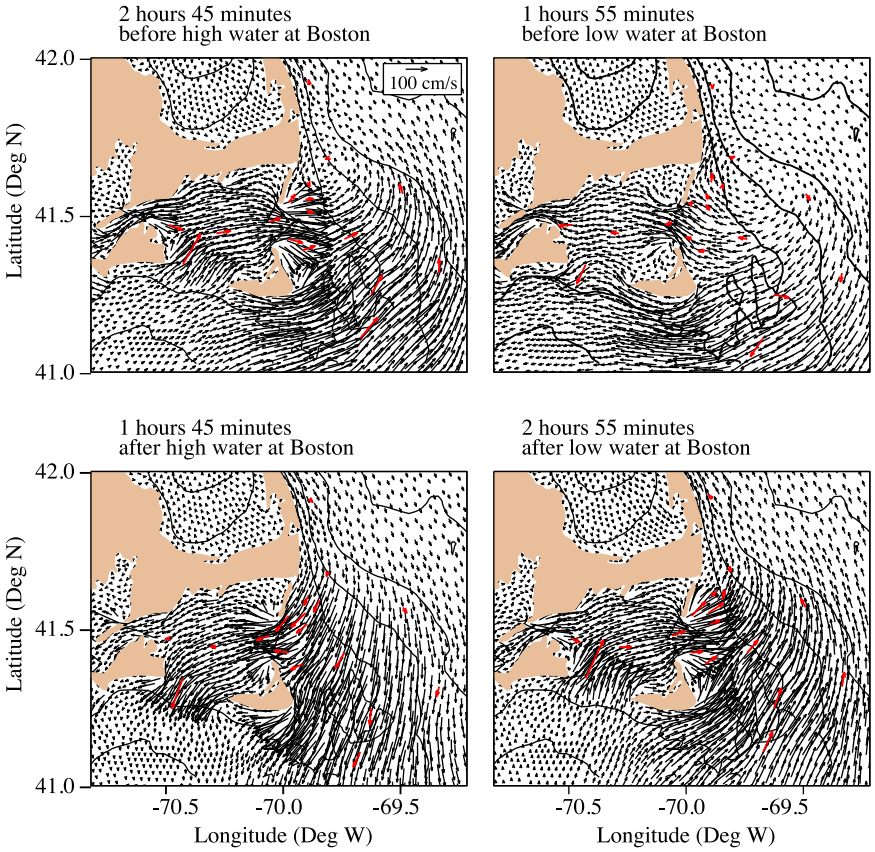

Figure 3. Time sequences showing the vertically averaged M_2 tidal current vectors in the Nantucket Sound and adjacent region during a tidal cycle relative to tidal elevation at Boston. Red vectors: observed currents shown by *Haight* [1942].

calculated through the assumption of mass conservation in the open boundary cell [*Chen et al.*, 2003]. Total numerical integration time for the tidal simulation was 90 days. In this study, the external time step was 12 s, and the ratio of the internal time step to the external time step was 10. The bottom stress was computed at each centroid assuming a logarithmic bottom boundary with a spatially varying bottom roughness length z_o. In the regions shallower than 40 m, z_o was set to 0.3 cm. This value of z_o was selected according to the best fit of the model-predicted vertical shear of the tidal current to observations made in the logarithmic layer on GB [*Werner et al.*, 2003; *Chen et al.*, 2001].

[10] The experiments were made for homogeneous and stratified conditions. For stratified cases, the model was forced by the same tidal forcing at the open boundary and run prognostically with the initial temperature and salinity fields specified using June and December hydrographic climatology, respectively. The tidal simulations have been compared with observed tidal elevation amplitudes and phases and current ellipse parameters at measurement sites available in the computational domain (Figure 1). Co-tidal charts of the five major tidal constituents were created using the harmonic constants predicted by FVCOM and field data. The empirical charts were constructed using the *Egbert and Erofeeva* [2002] inverse tidal model results. We will provide a brief summary of results for the homogeneous case over the regional scale and focus the remainder of the paper on new findings regarding the influence of stratification, energy budgets, and tidal dynamics over NES.

3. Simulation of Tidal Elevation and Currents

3.1. Homogeneous Case

[11] The general features of the tidal elevation in the GoM/GB/NES region are well known [*Garrett*, 1974; *Greenberg*, 1979; *Moody et al.*, 1984; *Brown*, 1984; *Daifuku and Beardsley*, 1983; *Brown and Moody*, 1987] and are captured by the high-resolution FVCOM simulations. A detailed model-data comparison is given in Appendix A. In the interior of the GoM, FVCOM-computed tidal currents obtain the same level of accuracy as previous tidal simulation results presented by *Lynch and Naimie* [1993] and

Table 1. Differences of Standard Deviations of Tidal Elevations and Phases With Comparison to Observations for the Cases With Homogeneous, June and December Stratified Conditions

Tidal Constituent	$\Delta\zeta_{June} - \Delta\zeta_h$ (cm)	$\Delta\theta_{June} - \Delta\theta_h$ (deg)	$\Delta\zeta_{Dec} - \Delta\zeta_h$ (cm)	$\Delta\theta_{Dec} - \Delta\theta_h$ (deg)
M_2	1.5	0.4	1.5	0.4
N_2	0.2	−0.3	0.3	−0.3
S_2	0.1	0.4	0.2	0.5
K_1	−0.3	0.1	−0.3	0.1
O_1	0.3	1.5	0.3	1.5

Table 2. Differences of the Standard Deviation of Tidal Current Ellipse Parameters With Comparison to Observations for the Cases With Homogeneous and June Stratified Conditions

Tidal Constituent	$\Delta U^s_{maj} - \Delta U^h_{maj}$ (cm/s)	$\Delta U^s_{min} - \Delta U^h_{min}$ (cm/s)	$\Delta\alpha^s_{min} - \Delta\alpha^h_{min}$ (deg)	$\Delta\theta^s_{min} - \Delta\theta^h_{min}$ (deg)
M_2	0.5	0.8	−3.3	−1.9
N_2	−0.2	0.0	−2.3	−4.1
S_2	0.5	0.3	−3.4	−2.1
K_1	−0.3	−0.3	−3.8	−1.7
O_1	0.2	−0.4	−2.7	−3.7

Chen et al. [2001]. The major improvement made by FVCOM is near the coast and in the Bay of Fundy and NES. For example, the spatial distribution of tidal currents in the Bay of Fundy is geometrically controlled, with ellipses paralleling local isobaths and the magnitude increasing toward the head of the Bay. Around Grand Manan Island, the tidal currents split at the southern end of the island and a zone of weak tidal currents exists on the northeastern side of the island. The maximum tidal currents are located in the narrowest area of Minas Channel, with a magnitude of over 3.5 m/s.

[12] It has long been recognized since the pioneering work of *Haight* [1942] that the phase of the M_2 tidal current in the eastern entrance to Nantucket Sound leads that of the adjacent western GoM and GB region (Figure 3). For example, the observed phase is 75° at Pollock Rip (69.900°W, 41.617°N) near the south end of Monomoy Island, but varies from 90° to 180° on GB. Even over Nantucket Shoals, the observed phase of the M_2 tidal current varies significantly in space. An example can be found by comparing the tidal current phases at Great Round Rip (69.917°W, 41.400°N) and Pollock Rip. Although the distance between these two sites is only ∼15 km, the phase at Great Round Rip leads that at Pollock Rip by 51°.

[13] The M_2 tidal current charts made by *Haight* [1942] relative to low and high waters at Boston and Pollock Rip show significant spatial variations in the tidal current direction in Nantucket Sound and the adjacent Great South Channel, Nantucket Shoals, and the western GoM. The difference in the M_2 tidal current direction at 10 m in the region east of Cape Cod and Nantucket Island and the 100-m isobath west of the Great South Channel can exceed 90° during the flood tide and even 180° during the ebb tide (during flood, water flows out of Nantucket Sound into the Great South Channel; during ebb, water flows into Nantucket Sound from the Great South Channel). Due to the very limited number of measurement sites available to *Haight* [1942] his tidal charts do not provide sufficient spatial detail to interpret his measurements.

[14] To aid comparison, we digitized the tidal current vectors in *Haight*'s [1942, Figures 23–32] charts and superimposed them on the model current fields at different stages of the M_2 tide relative to Boston. The resulting current maps (Figure 3) show good agreement and nicely illustrate the tidal flushing process in Nantucket Sound and the adjacent regions. During flood, water enters Nantucket Sound from the west through Vineyard Sound and from the south between Martha's Vineyard and Nantucket Island and then flows eastward out of Nantucket Sound between Cape Cod and Nantucket Island (Figure 3, top left). This current pattern is reversed during ebb (Figure 3, top right). East of Monomoy, a cyclonic eddy forms when the water moves across isobaths and into the deeper Great South Channel during flood. This eddy is clearly evident at 2 h 45 min before high water at Boston (Figure 3, top left). In turn, an anti-cyclonic eddy appears just west of Monomoy after the maximum ebb tidal current, as evident at 1 h 55 min before low water at Boston (Figure 3, top right). The high spatial variability that Haight and others have reported in the phase of the M_2 tidal currents near Pollock Rip east of Monomoy Island is in part a result of eddy formation during flood and ebb flow.

[15] With better resolution of coastal geometry in Nantucket Sound, FVCOM captures the multiscale tidal flushing process around the islands, which provides an explanation for the phase leading phenomenon at Pollock Rip relative to the NES and GoM - a curiosity that was suggested by the observations of *Haight* [1942] but has not been resolved until this study. The model-predicted cyclonic and anti-cyclonic eddies east of Monomoy Island after maximum flood and ebb tidal flows can be simply explained by the potential vorticity conservation law in the form of

$$q = \frac{\zeta + f}{H} = \text{constant}, \tag{1}$$

where ζ is the relative vorticity, f the Coriolis parameter, and H is the local water depth. For a column starting at depth H_o with relative vorticity ζ_o, its relative vorticity is given by

$$\zeta = \zeta_o \frac{H}{H_o} + f(H - H_o)/H_o. \tag{2}$$

[16] The first term on the right is the change associated with the column's initial relative vorticity while the second term is due to conservation of planetary vorticity. A column with initial cyclonic (anticyclonic) vorticity moving into deeper water will gain cyclonic (anticycolonic) vorticity (first term) and cyclonic vorticity (second term). The currents in the Nantucket Sound region have sufficient shear that both terms can be important, with the first term becoming dominant in the Monomoy-Nantucket Island gap region. This process favors the formation of the cyclonic (anticyclonic) eddy east (west) of Monomoy during the flood (ebb) tidal stage.

3.2. Stratified Case

[17] Stratification in the GoM varies with season, strongest during summer and weakest during winter [*Hopkins and Garfield*, 1979; *Mountain and Jessen*, 1987; *Brown and Irish*, 1993; *Loder et al.*, 2001; *Smith et al.*, 2001].

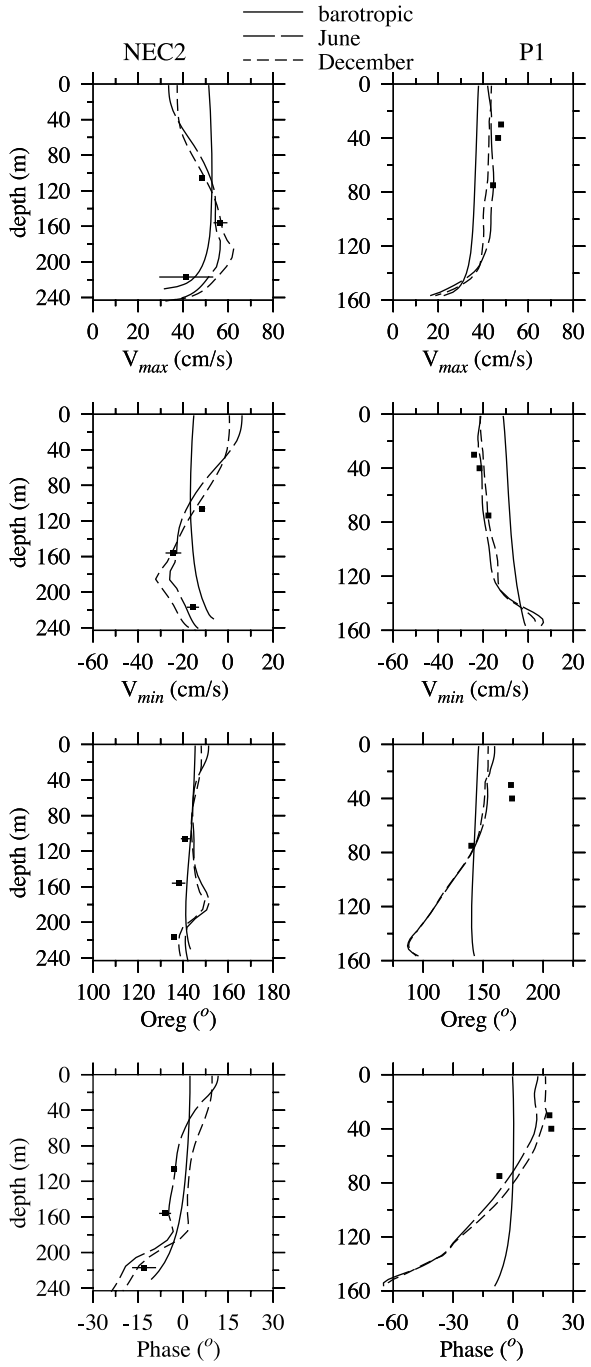

Figure 4. Comparison between model and observed amplitudes of tidal currents at stations labeled NEC2 and P1 in the work by *Moody et al.* [1984] for homogeneous, June, and December stratification conditions. Dots denote the observed amplitudes and horizontal lines through dots represent measurement uncertainty. The definitions of lines are given in the legend.

Separate tidal simulations were run with climatologically averaged June and December stratification for initial conditions, and comparisons were made to examine the difference in tidal elevation and currents at measurement sites. The results show that including summertime and wintertime stratification causes a minor change in tidal amplitude of order ~1.5 cm for M_2, 0.1–0.3 cm for N_2 and S_2, and ~0.3 cm for K_1 and O_1 (Table 1). This is also true for tidal phase, which shows a maximum difference ~1.5°. This means that the contribution of stratification to the tidal elevation around the coast is negligible.

[18] Similar results are also found for tidal currents. Table 2 shows the difference of the standard deviations of tidal currents between homogenous and June stratification cases. For M_2 tide, for example, including stratification only causes an overall change of 0.5 cm/s for major axis, 0.8 cm/s for minor axis, 3.3° for orientation and 1.9° for phase. This result, however, needs to be interpreted with caution. Stratification does cause a significant influence on the vertical profile of tidal currents, even though its overall contributions to the standard deviation of tidal simulation results at measurement site and depth is small. An example is given in Figure 4, which shows vertical profiles of the comparison of model and observed tidal currents for homogeneous, June and December stratification cases. At NEC2 in the Northeast Channel (42.300°N, 65.967°W), the model-computed tidal velocity for the stratified case features a second-mode structure with a maximum amplitude around a depth of ~180 m, which is quite different from that predicted for the homogeneous case. The maximum tidal velocity found around a depth of ~170 m is probably related to the existence of Marine Intermediate Water (MIW), which forms as a result of surface cooling during winter and surface heating during spring through summer [*Brown and Beardsley*, 1978; *Hopkins and Garfield*, 1979; *Chen et al.,* 1995]. At PI on the northern edge of GB (42.200°N, 67.250°W), including stratification significantly improves the simulation accuracy. In addition to a better match with the data, the model-predicted tidal velocities in the stratified cases suggest a large phase difference in the vertical, which was not resolved in the homogeneous case. At this site, the fact that the tidal velocity is significantly underestimated in the homogeneous case suggests the presence of internal tides that contribute directly to the total tidal energy.

[19] To examine the contribution of stratification to tides in the GoM, we estimated the total M_2 tidal energy flux into a closed box covering this region and into selected subregions of the GB, western shelf of Nova Scotia, BF, and Nantucket Sound/Shoals in the regional box. The total tidal energy flux is defined as

$$\vec{E} = \left\langle \int_{-H}^{\zeta} \left[\rho \vec{v} D \left(\frac{u^2 + v^2}{2} \right) + g\zeta \right] dz \right\rangle, \tag{3}$$

where $\vec{E}$ is the tidal energy flux per unit width, $\vec{v}$ is the tidal velocity vector with x and y components of u and v, D is the total water depth, ζ is the tidal elevation, ρ is the water density, and g is gravity. The angled bracket denotes a time average over a tidal period (T) [*Crawford*, 1984; *Chen et al.*, 2009]. To quantify the contribution of internal tides, we estimated the M_2 internal tidal energy flux defined as

$$\vec{M}_{bc} = \langle \vec{v}_{bc} p_{bc} \rangle \tag{4}$$

where p_{bc} is the hydrostatic, baroclinic pressure associated with the M_2 tidal motion and $\vec{v}_{bc} = \vec{v}_h - \vec{v}_{bt}$ is defined as the

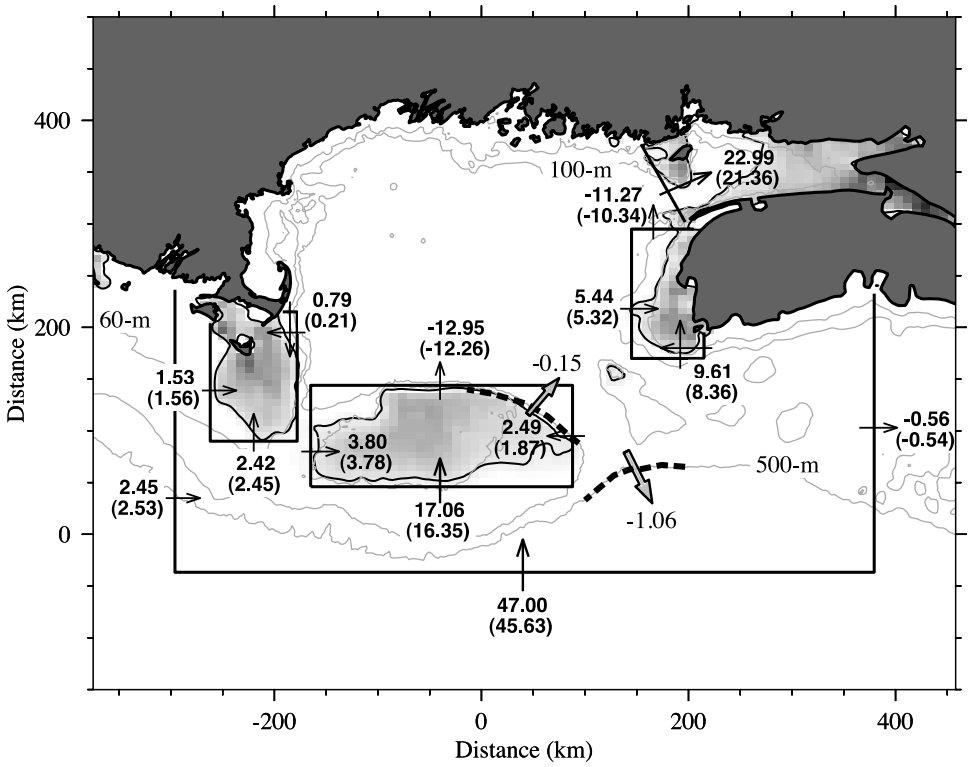

Figure 5. Sectionally integrated M_2 energy fluxes (in GW) for homogeneous (bold) and June stratification (bold in parentheses) cases. Arrows indicate the inflow and outflow fluxes. Dashed lines are the sections where the internal M_2 energy flux for the June stratification case (in GW) is estimated. Number on the tip of a filled arrow is the flux for the internal M_2 tide. The gray colored areas are tidally well-mixed zones bounded by a heavy line of $\log_{10}(h/D_t) = 2.1$. In these areas, $\log_{10}(h/D_t) \leq 2.1$, with a gray scale ranging from 0 (black) to 2.3 (white).

baroclinic tidal velocity in which $\vec{v}_h$ is the horizontal velocity field and $\vec{v}_{bt}$ is the depth-averaged barotropic component of the horizontal velocity [*Cummins and Oey*, 1997]. The depth-integrated internal tidal energy flux vectors are estimated by

$$\vec{J}_{bc} = \int_{-H}^{\zeta} \vec{M}_{bc} dz. \tag{5}$$

[20] The total M_2 tidal energy flux is presented in Figure 5. Gray shaded areas are the tidally well-mixed zones bounded by the front defined by $log_{10}(h/D_t) = 2.1$, where D_t is the tidal energy dissipation rate [*Simpson and Hunter*, 1974; *Loder and Greenberg*, 1986; *Chen et al.*, 1995, 2001]. The net flux entering the boundary of the regional (largest) box is 48.89 GW for the homogeneous case and 47.62 GW (a 2.6% reduction) for the June stratification case. GB, the western shelf of Nova Scotia, BF, and Nantucket Sound/Shoals are the four largest tidal dissipation areas in the GoM/GB/NES domain. GB and the western shelf of Nova Scotia are tidal energy flow-through areas in which the inflow tidal energy flux is much larger than the outflow tidal energy flux, while the BF and Nantucket Sound/Shoals are tidal energy sinks with only inflow flux. In the homogeneous case, the net flux (inflow flux minus outflow flux) is 10.4 GW on GB and 3.78 GW on the western shelf of Nova Scotia. Including June stratification does not change the features observed in the homogeneous case in these two areas. The net flux difference for homogeneous and June stratified cases is 0.66 GW on GB and 0.44 GW on the western shelf of Nova Scotia, which account for 6.35% and 11.64% of the net tidal energy fluxes, respectively. The tidal energy flux is 22.99 GW into the BF and 4.74 GW into Nantucket Sound/Shoals for the homogeneous case. The flux differences between homogeneous and June stratification cases are 1.63 GW for the BF and 0.52 GW for Nantucket Sound/Shoal, which account for only 7% and 11% of the inflow tidal energy flux in these two areas, respectively. Comparing the flux into the BF with that at the outside boundary of the GoM and NES, about 47% of the total tidal energy flux from the open ocean enters the BF.

[21] The internal tidal energy flux estimated using (5) clearly shows two energetic areas: *a*) the northeastern flank of GB where the isobaths separate and the along- and cross-bank residual currents diverge [*Chen et al.*, 2001] and *b*) in the Northeast Channel, a major energy passage into the GoM. The total baroclinic tidal energy flux across the sections (shown as segments of the 100-m isobath on the northeast flank of GB and 500-m isobath in the Northeast Channel) is 0.15 GW on the northeast flank and 1.06 GW in the Northeast Channel. These values are orders of magnitude smaller than the barotropic tidal energy flux.

[22] Assuming that the net tidal energy flux is balanced by tidal dissipation, we can estimate the dissipation rate in the GoM. For the homogenous case, the dissipation rate should be 48.9 GW for the GoM, 10.4 GW on GB, 3.8 GW on the

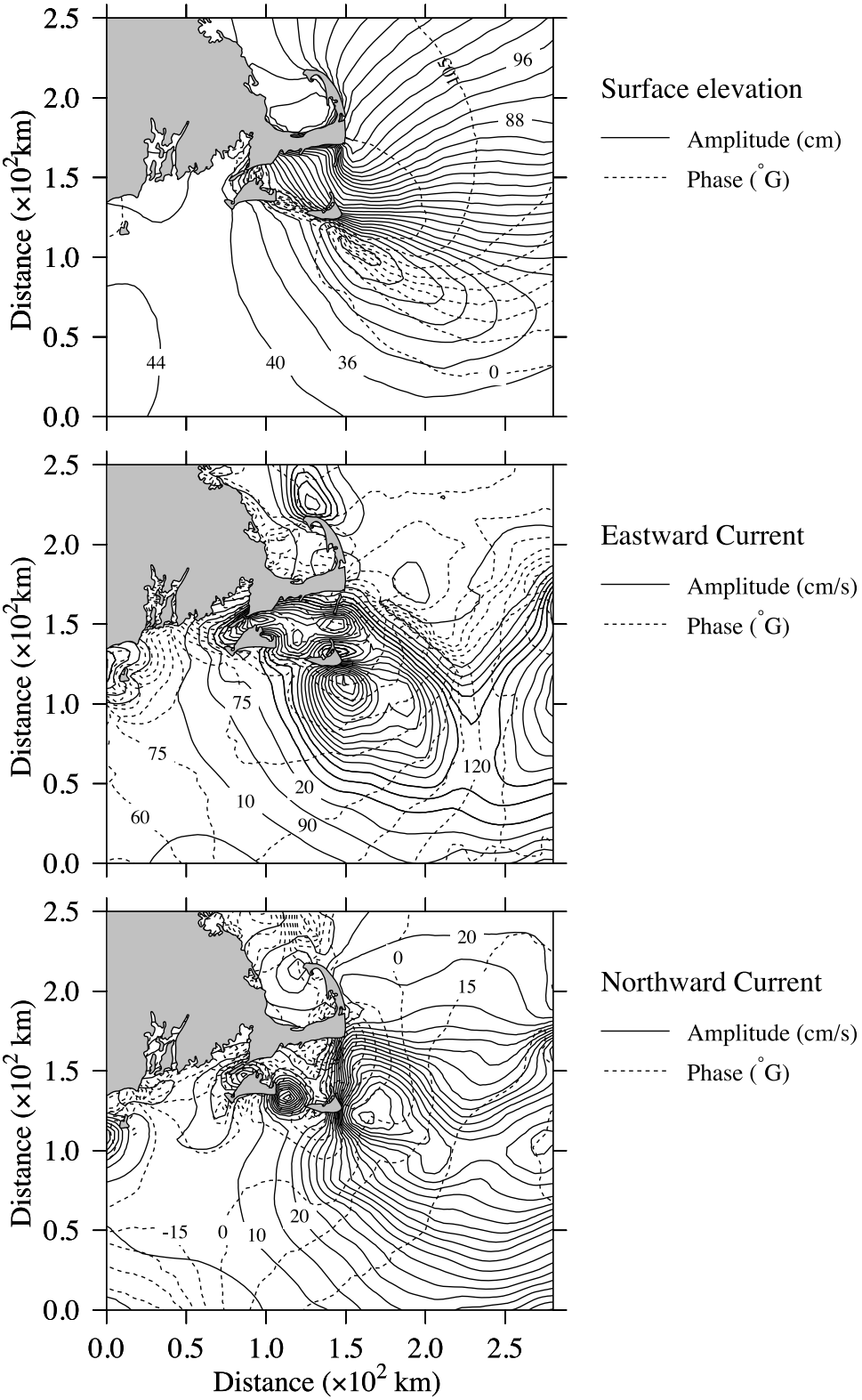

Figure 6. Distributions of the M_2 tidal amplitude (solid line) and phase (dashed line) over the New England shelf, Nantucket Sound/Shoals, and east of Cape Cod for (top) surface elevation, (middle) eastward current, and (bottom) northward current.

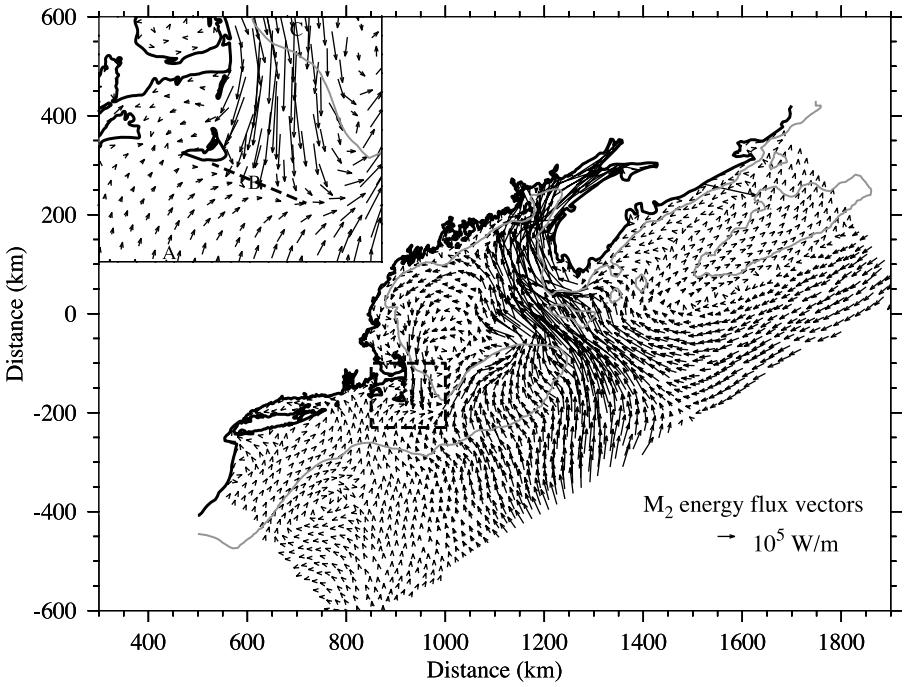

Figure 7. Map of the M_2 tidal energy flux vectors in the GoM/GB/NES region. The inset shows an enlarged view for the Nantucket Shoals area. Sites A, B and C are the locations where the momentum balance results are presented in Figure 8. Units: 10^5 W/m^2.

western shelf of Nova Scotia, 23.0 GW in the BF, and 4.8 GW in Nantucket Sound/Shoals. These four tidally well-mixed regions account for 85.9% of the total dissipation in the GoM, in which the BF accounts for 47% of total dissipation. For the summertime stratification case, the dissipation rates in these regions are 47.2 GW, 9.7 GW, 3.3 GW, 21.4 GW and 4.2 GW, respectively, with the same order of the ratios as those for the homogeneous case.

[23] The tidal energy dissipation rate also can be estimated directly using the stress and tidal velocity at the bottom [*Simpson and Hunter*, 1974; *Foreman et al.*, 2000] in the form given as

$$D_t = -\frac{1}{T}\int_0^T \rho \vec{u}_b \cdot \vec{\tau}_b dt \qquad (6)$$

where T is the tidal period, $\vec{u}_b$ is the bottom velocity and $\vec{\tau}_b$ is the bottom stress. This formulation omits two low order of terms described by *Gill* [1982] and *Zhong and Li* [2006]. Considering the M_2 tidal constituent, the total dissipation rate over a specified area Ω equals the integration of (6) over Ω. Using the model computed $\vec{u}_b$ and $\vec{\tau}_b$ with ρ = 1025 kg m^{-3}, we estimated the total dissipation over the GoM and four tidally well-mixed regions for the homogenous case. They are 48.6 GW for the GoM, 10.0 GW on GB, 3.6 GW in the western shelf of Nova Scotia, 21.2 GW in the BF, and 4.7 GW in Nantucket Sound/Shoals, respectively. These values are similar to those estimated by the net tidal energy fluxes described above. The difference between these two methods (0.6% for the GoM, 3.9% for GB, 5.3% for the western shelf of Nova Scotia, 7.8% for the BF and 2.1% for Nantucket Sound/Shoal) may be attributed to omitting terms in the frictional dissipation expression and errors in numerical integration.

[24] The tidal energy flux in the GoM under homogenous conditions was estimated in previous tidal studies, with a major focus on the dissipation rate of the BF [*Jeffreys*, 1921; *McLellan*, 1958; *Godin*, 1969; *Garrett*, 1972; *Greenberg*, 1979]. The estimated dissipation rate over one tidal cycle in the BF ranged from 19 GW to 55 GW. The tidal dissipation value of 23 GW (estimated by a net tidal energy flux) and 21.2 GW (estimated by the frictional dissipation expression) from our high-resolution FVCOM simulation is consistent with those studies, even though our interests here are aimed at estimating the contribution of stratification to the tidal energy flux.

4. Tidal Dynamics Over the NES

[25] Based on long-term (~one year) moored current measurements made west of Nantucket Shoals, *Shearman and Lentz* [2004] described the barotropic tidal variability over the eastern NES. They found that the M_2 surface elevation decreased toward the northeast and reached a minimum over Nantucket Shoals, while the depth-averaged tidal current amplitude increased toward the northeast and reached a maximum near Nantucket Island. *Shearman and Lentz* [2004] also used their in situ data to examine the depth-averaged tidal momentum balance over the eastern NES, and found it to be essentially linear, with a balance between the local acceleration, Coriolis force and surface pressure gradient in both along- and cross-isobath directions.

[26] FVCOM-predicted tidal elevation and current amplitudes are in good agreement with the in situ measurements

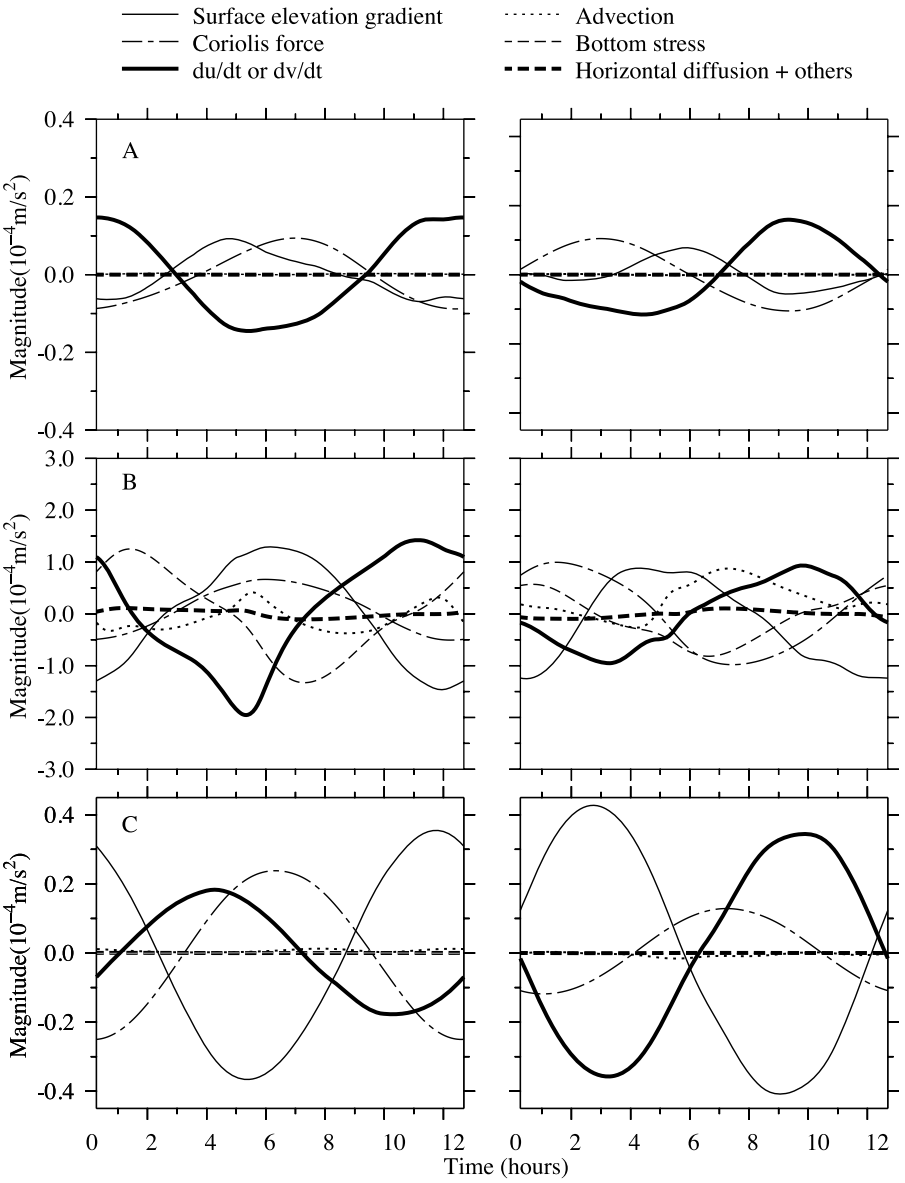

Figure 8. Balance of the (left) *x* (eastward) and (right) *y* (northward) momentum equations at select sites: site A, east of Cape Cod; site B, within the convergence zone; and site C, over the NES. Locations of sites A, B and C are shown in Figure 7.

and analysis presented by *Shearman and Lentz* [2004]. The model reproduces the northeastward decrease in M_2 tidal elevation and divergence in the tidal current amplitude over the NES toward Martha's Vineyard and Nantucket Island (Figure 6). In addition, the model results show a southward decrease in M_2 elevation along the east coast of Cape Cod to Nantucket Island, which is also consistent with the southward divergence of the tidal current amplitude in that region. A narrow zone of minimum tidal elevation amplitude forms southeast of Nantucket Island, with an orientation in the northwest-southeast direction. The maximum east currents occur just west of this zone and maximum north currents occur just north of this zone.

[27] The model M_2 elevation and currents have been used to compute the tidal energy flux for the model domain. The distribution of flux vectors clearly shows that tidal energy enters the GoM from the open ocean off GB, the Northeast Channel, and western Scotian Shelf (Figure 7). A large fraction of this energy propagates into the BF, while the rest turns counterclockwise and propagates west- to southwestward along the western GoM toward Cape Cod. An energy convergence zone is found southeast of Nantucket Island with a northwest-southeast orientation where the southward-propagating tidal energy flux from the western GoM along Cape Cod meets the northeastward tidal energy flux from the eastern NES. This pattern indicates an interaction between tidal waves propagating into this zone from the GoM and NES. The phase difference between these two waves results in the formation of the minimum surface elevation and energy convergence zones southeast of Nantucket Island.

[28] To examine the local dynamics of these two waves, a simple momentum balance analysis was made using the

Table A1. Statistics of the Comparison Between Model-Computed and Observed Tidal Elevations at Tidal Measurement Sites

Tidal Constituent	Observed Elevation Mean (cm)	Model-Data Elevation Difference STD (cm)	Data Error STD (cm)	Model-Data Phase Difference STD (deg)	Data Error STD (deg)
M_2	62.39	3.21	0.77	3.45	0.75
N_2	13.81	1.93	0.65	7.00	1.31
S_2	11.71	1.55	0.31	4.35	1.47
K_1	9.48	1.33	0.56	4.28	3.53
O_1	7.50	0.71	0.41	4.29	3.75

model solution. East of Cape Cod and southwest of Nantucket Island, these two waves exhibit essentially linear dynamics, with a balance between local acceleration, Coriolis force and surface pressure gradient in the east (x) and north (y) directions (Figure 8). Nonlinear advection and bottom stress terms are too small to contribute significantly in the momentum balance. This result agrees with the results of *Shearman and Lentz* [2004] for the tidal wave propagating northeastward over the NES, suggesting that FVCOM has correctly captured the dynamics in that region.

[29] The dynamics becomes more complex in the region where these two waves meet southeast of Nantucket Island (Figure 8, middle). In the overlapping zones of minimum surface elevation and energy flux convergence, the nonlinear advective terms become significant, indicative of energy transfer from tidal motion to residual flow, and the bottom stress term increases dramatically, providing a strong local tidal energy sink. Part of this dissipation results in the sediment resuspension and vertical turbulent mixing that occurs over Nantucket Shoals.

5. Summary

[30] This paper investigates the dominant tides in the GoM and adjacent shelf region using FVCOM. The model captures the near-resonance nature of the M_2 tidal wave in the BF/GoM system first described by *Garrett* [1972], and the complex dynamics in the transition zone between the GoM and the eastern NES described by *Shearman and Lentz* [2004].

[31] Experiments with climatologically averaged June and December initial stratification show minor change in tidal elevation. However, stratification significantly influences the vertical structure of the tidal currents. Tidal energy flux analysis shows that the semidiurnal tidal energy enters the GoM mainly through the Northeast Channel. GB and the western shelf of Nova Scotia are tidal energy flow-through systems characterized by large tidal dissipation. In these two systems, the inflow tidal energy is much larger than the outflow tidal energy. The BF and Nantucket Sound/Shoals are tidal energy sinks where only inflow energy flux occurs. Internal tides are energetic in the stratified regions over steep bottom topography and in the Northeast Channel, but its contribution to the total tidal energy flux are orders of magnitude smaller than the homogeneous tides. The model suggests that the tidal flushing-induced eddy shedding around islands and headlands is the dynamic basis for the observed phase lead of the M_2 tide over the slope between Cape Cod and Nantucket Island. A minimum sea level zone along a southeast-oriented line from Nantucket Island forms as a results of the interaction of the southward propagating tidal wave in the region east of Cape Cod and the northeastward propagating tidal wave from NES south of the Nantucket Island.

Appendix A: Comparisons With Tidal Measurements

[32] A total of 98 tidal gauge and bottom pressure measurements for tidal elevation and 130 sites (with 278 time series records at various depths) for tidal currents were used to validate the model simulation. To maintain brevity of the manuscript, we do not include a detailed comparison in this appendix. A summary of statistics is given in Table A1 for tidal elevation and phase and Table A2 for tidal current ellipse parameters. Subtracting measurement uncertainties, standard deviations of the model-computed and observed amplitude difference accounts for 4, 10, 10, 8 and 4% errors relative to the mean tidal elevation over 98 sites for the M_2, N_2, S_2, K_1 and O_1, constituents respectively. Similarly, the standard deviation of the model-computed and observed phase difference is about 5.6, 11.8, 5.8, 3.0, and 2.4 min for these five tidal constituents, respectively. It should be pointed out that many tidal gauges are located at sites close to or within rivers and inlets with complex bathymetry and coastal geometry. Tidal motion at those stations will be influenced by estuarine/shelf interactions, which have not been included in the current study.

Table A2. Statistics of the Comparison Between Model-Computed and Observed Tidal Current Ellipse Parameters

Tidal Constituent	Model-Data Major Axis Difference STD (cm/s)	Observed Major Axis Error STD (cm/s)	Model-Data Minor Axis Difference STD (cm/s)	Observed Minor Axis Error STD (cm/s)	Model-Data Orientation Difference STD (deg)	Observed Orientation Error STD (deg)	Model-Data Phase Difference STD (deg)	Observed Phase Error STD (deg)
M_2	4.1	1.5	3.6	0.9	15.7	21.6	14.4	18.9
N_2	2.1	0.8	1.3	0.6	17.1	24.3	17.2	21.1
S_2	1.2	0.6	0.8	0.5	19.5	26.6	16.8	26.7
K_1	1.7	0.7	1.3	0.4	21.8	30.5	19.6	26.5
O_1	1.3	0.4	1.1	0.3	21.9	29.7	17.4	23.8

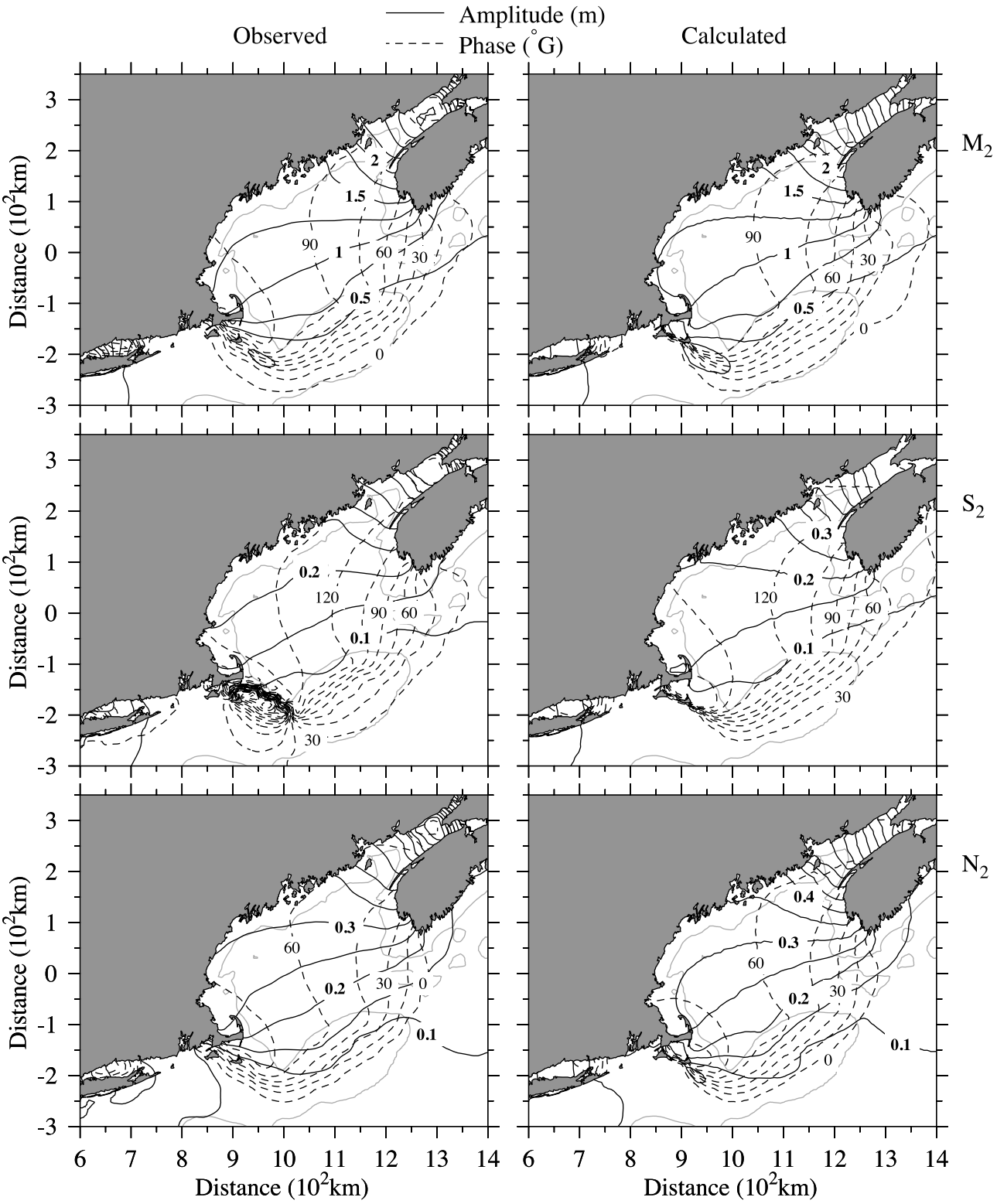

Figure A1. Comparison between (left) observed and (right) model co-tidal charts for the semidiurnal (M_2, S_2, and N_2) tidal elevations. Co-amplitude (m) and co-phase (°G) lines are plotted every 0.25 m and 15° G, respectively.

[33] *Egbert and Erofeeva* [2002] used an inverse data assimilation approach to incorporate all types of tidal data into a regional finite difference tidal model and created a database of tidal constants with a horizontal resolution of 1/6° in the North Atlantic Ocean. This database was used to construct observed co-tidal charts of M_2, N_2, S_2, and O_1 and K_1 tidal constituents in the GoM/GB region. Without data assimilation, FVCOM accurately reproduced the observed

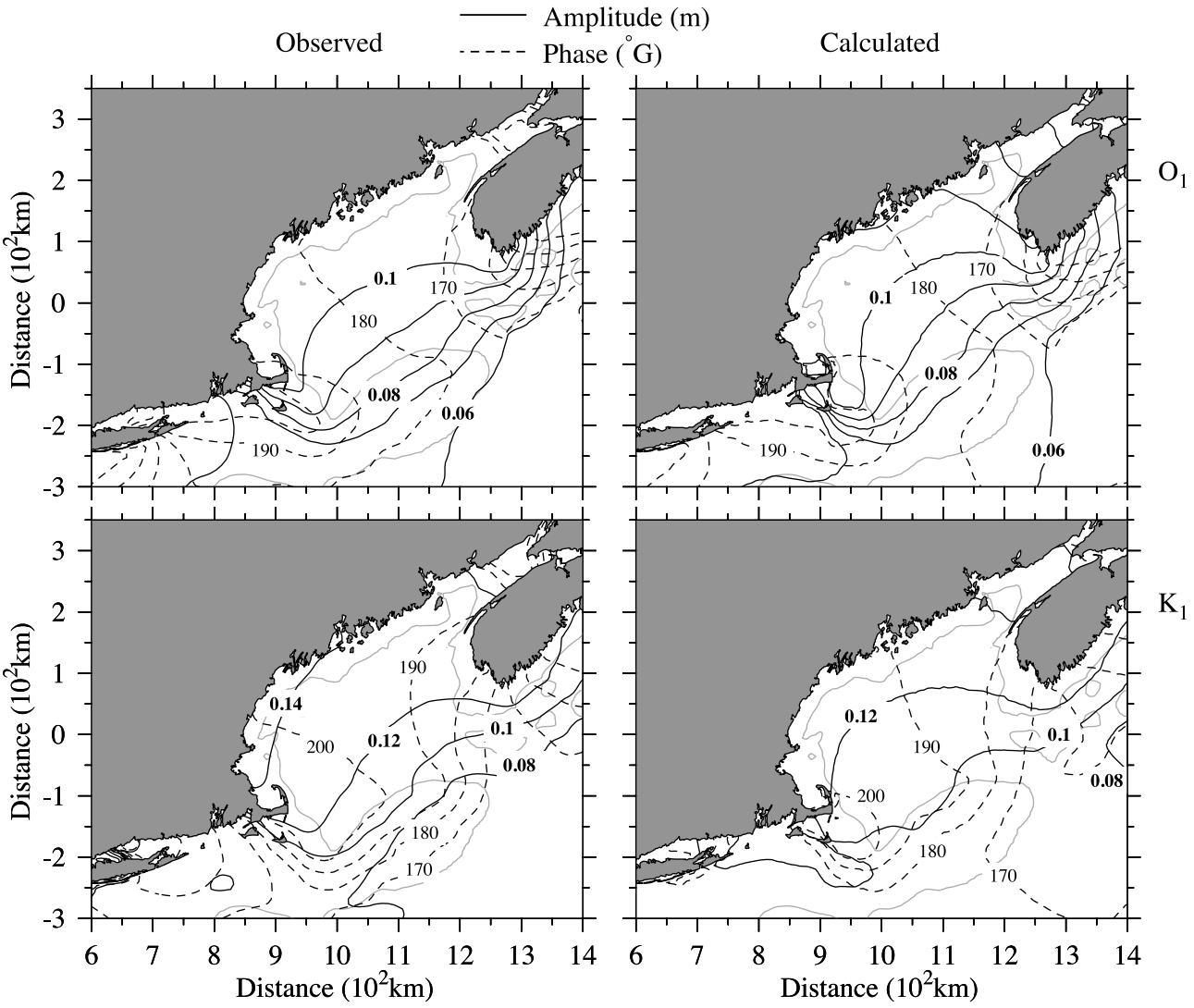

Figure A2. Comparison between (left) observed and (right) model co-tidal charts for diurnal (K_1 and O_1) tidal elevations. Co-amplitude (m) and co-phase (°G) lines are plotted every 0.02 m and 10° G, respectively.

distributions of co-amplitude and co-phase of the resonance M_2 tidal constituent in the computational region (Figure A1). The model-predicted distributions of co-amplitudes and co-phases of N_2, S_2, K_1 and O_1 are also in good agreement with the distributions constructed using the tidal inverse model (Figure A2).

[34] Ellipse parameters (major axis, minor axis, orientation, and phase) of the five major tidal currents were calculated using the model-predicted 30-day time series of current output after the first 10-day period from model spin up. The model-data major and minor difference standard deviations are generally larger than measurement uncertainty standard deviations, but the model-data orientation and phase difference standard deviations are significantly smaller than the measurement uncertainty standard deviations (Table A2).

[35] In the open region, FVCOM-computed tidal currents show the same accuracy as previous tidal simulation results presented by *Lynch and Naimie* [1993] and *Chen et al.* [2001]. The major improvement made by FVCOM is near the coast and in the BF and NES. For example, the spatial distribution of tidal currents in the BF is geometrically controlled, with ellipses paralleling local isobaths and the magnitude increasing toward the head of the bay. Around Grand Manan Island, the tidal currents split at the southern end of the island and a zone of weak tidal currents exists on the northeastern side of the island. The maximum tidal currents are located in the narrowest area of Minas Channel, with a magnitude of over 3.5 m/s.

[36] **Acknowledgments.** This research is supported by the U.S. GLOBEC Northwest Atlantic/Georges Bank Program NSF (OCE-0234545, 0227679, 0606928, 0726851 and 0814505) to Changsheng Chen and Qixchun Xu and NSF grant (OCE-02-27679) and the WHOI Smith Chair to Robert Beardsley and Richard Limeburner. The tidal model-data comparison on Nantucket Sound/Shoals is partially the result of research sponsored by the MIT Sea Grant College Program, under NOAA grant NA06OAR4170019, MIT SG project 2006-R/RC-102, 2006-R/RC-103, 2006-R/RC-102, 2006-R/RC-107, 2008-R/RC-107), 2010-R/RC-116 and the NOAA NERACOOS Program for the UMASS team. C. Chen's contribution is also supported by Shanghai Ocean University International Cooperation Program (A-2302-11-0003), the Program of Science and Technology Commission of Shanghai Municipality (09320503700), the Leading Academic Discipline Project of Shanghai Municipal Education

Commission (project J50702), and Zhi jiang Scholar and 111 project funds of the State Key Laboratory for Estuarine and Coastal Research, East China Normal University (ECNU). The numerical experiments were conducted using the High Performance Computer Cluster of the Marine Ecosystem Dynamics Modeling Laboratory at the School of Marine Science and Technology, University of Massachusetts–Dartmouth, purchased through Massachusetts Marine Fisheries Institute NOAA grants DOC/NOAA/NA04NMF4720332 and DOC/NOAA/NA05NMF4721131. We thank Steve Lentz for his suggestion to use the FVCOM model results to examine the tidal dynamics on the New England Shelf and David Greenberg for his comments on the tidal simulation in the Bay of Fundy. This paper is U.S. GLOBEC contribution 714.

References

Beardsley, R. C., H. Mofjeld, M. Wimbush, C. N. Flagg, and J. J. Vermersch Jr. (1977), Ocean tides and weather-induced bottom pressure fluctuations in the Middle-Atlantic Bight, *J. Geophys. Res.*, *82*, 3175–3182, doi:10.1029/JC082i021p03175.

Bigelow, H. B. (1927), Physical oceanography of the Gulf of Maine, *U.S. Bur. Fish. Doc.*, *969*, pp. 511–1027, U.S. Govt. Print. Off., Washington, D. C.

Brown, W. S. (1984), A comparison of Georges Bank, Gulf of Maine and New England Shelf tidal dynamics, *J. Phys. Oceanogr.*, *14*, 145–167, doi:10.1175/1520-0485(1984)014<0145:ACOGBG>2.0.CO;2.

Brown, W. S., and R. C. Beardsley (1978), Winter circulation in the western Gulf of Maine. Part I: Cooling and water mass formation, *J. Phys. Oceanogr.*, *8*, 265–277, doi:10.1175/1520-0485(1978)008<0265:WCITWG>2.0.CO;2.

Brown, W. S., and J. D. Irish (1993), The annual variation of water mass structure in the Gulf of Maine 1986–1987, *J. Mar. Res.*, *51*, 53–107, doi:10.1357/0022240933223828.

Brown, W. S., and J. A. Moody (1987), Tides, in *Georges Bank*, edited by R. H. Backus and D. W. Bourne, pp. 100–107, MIT Press, Cambridge, Mass.

Chen, C., R. C. Beardsley, and R. Limeburner (1995), Variability of water properties in late spring in the northern Great South Channel, *Cont. Shelf Res.*, *15*(4–5), 415–431, doi:10.1016/0278-4343(94)00054-Q.

Chen, C., R. C. Beardsley, and P. J. S. Franks (2001), A 3-D prognostic model study of the ecosystem over Georges Bank and adjacent coastal regions. Part I: Physical model, *Deep Sea Res.*, *48*, 419–456, doi:10.1016/S0967-0645(00)00124-7.

Chen, C., H. Lui, and R. C. Beardsley (2003), An unstructured, finite-volume, three-dimensional, primitive equation ocean model: Application to coastal ocean and estuaries, *J. Atmos. Oceanic Technol.*, *20*, 159–186, doi:10.1175/1520-0426(2003)020<0159:AUGFVT>2.0.CO;2.

Chen, C., R. C. Beardsley, and G. Cowles (2006a), An unstructured grid, finite-volume coastal ocean model (FVCOM) system, *Oceanography*, *19*(1), 78–89.

Chen, C., R. C. Beardsley, and G. Cowles (2006b), An unstructured grid, finite-volume coastal ocean model-FVCOM user manual, second edition, *Tech. Rep. SMAST/UMASSD-06-0602*, 318 pp., Sch. for Mar. Sci. and Technol., Univ. of Mass-Dartmouth, New Bedford.

Chen, C., H. Huang, R. C. Beardsley, H. Liu, Q. Xu, and G. Cowles (2007), A finite-volume numerical approach for coastal ocean circulation studies: Comparisons with finite difference models, *J. Geophys. Res.*, *112*, C03018, doi:10.1029/2006JC003485.

Chen, C., G. Gao, J. Qi, A. Proshutinsky, R. C. Beardsley, Z. Kowalik, H. Lin, and G. Cowles (2009), A new high-resolution unstructured-grid finite-volume Arctic Ocean model (AO-FVCOM): An application for tidal studies, *J. Geophys. Res.*, *114*, C08017, doi:10.1029/2008JC004941.

Clarke, A. J. (1991), The dynamics of barotropic tides over the continental shelf and slope (review), in *Tidal Hydrodynamcs*, edited by B. B. Parker, pp. 79–108, John Wiley, New York.

Crawford, W. R. (1984), Energy flux and generation of diurnal shelf waves along Vancouver Island, *J. Phys. Oceanogr.*, *14*, 1600–1607, doi:10.1175/1520-0485.

Cummins, E., and L. Y. Oey (1997), Simulation of barotropic and baroclinic tides off northern British Columbia, *J. Phys. Oceanogr.*, *27*(5), 762–781, doi:10.1175/1520-0485(1997)027<0762:SOBABT>2.0.CO;2.

Daifuku, P. R., and R. C. Beardsley (1983), The K1 tide on the continental shelf from Nova Scotia to Cape Hatteras, *J. Phys. Oceanogr.*, *13*(1), 3–17.

Egbert, G. D., and S. Y. Erofeeva (2002), Efficient inverse modeling of barotropic ocean tides, *J. Atmos. Oceanic Technol.*, *19*(2), 183–204, doi:10.1175/1520-0426(2002)019<0183:EIMOBO>2.0.CO;2.

Foreman, M. G. G., W. R. Crawford, J. Y. Cherniawsky, R. F. Henry, and M. R. Tarbotton (2000), A high-resolution assimilating tidal model for the northeast Pacific Ocean, *J. Geophys. Res.*, *105*, 28,629–28,651, doi:10.1029/1999JC000122.

Garrett, C. (1972), Tidal resonance in the Bay of Fundy and Gulf of Maine, *Nature*, *238*, 441–443, doi:10.1038/238441a0.

Garrett, C. (1974), Normal modes of the Bay of Fundy and Gulf of Maine, *Can. J. Earth Sci.*, *11*, 549–556, doi:10.1139/e74-049.

Gill, A. E. (1982), *Atmosphere–ocean Dynamics*, *Int. Geophys. Ser.*, vol. 30, Academic, San Diego, Calif.

Godin, G. (1969), Theory of exploration of tidal energy and its application to the Bay of Fundy, *J. Fish. Res. Board Can.*, *26*, 2887–2957, doi:10.1139/f69-281.

Greenberg, D. A. (1979), A numerical model investigation tidal phenomena in the Bay of Fundy and Gulf of Maine, *Mar. Geod.*, *2*, 161–187, doi:10.1080/15210607909379345.

Greenberg, D. A. (1983), Modeling the mean barotropic circulation in the Bay of Fundy and Gulf of Maine, *J. Phys. Oceanogr.*, *13*, 886–904, doi:10.1175/1520-0485(1983)013<0886:MTMBCI>2.0.CO;2.

Haight, F. J. (1942), Coastal currents along the Atlantic coast of the United States, *Spec. Publ.*, *239*, 73 pp., Coastal and Geodetic Survey, U.S. Dep. of Commer., Washington, D. C.

Hopkins, T. S., and N. Garfield III (1979), Gulf of Maine Intermediate Water, *J. Mar. Res.*, *37*, 103–139.

Hubbard, M. E. (1999), Multidimensional slope limiters for MUSCL-type finite volume schemes on unstructured grids, *J. Comput. Phys.*, *155*, 54–74, doi:10.1006/jcph.1999.6329.

Jeffreys, H. (1921), Tidal friction in shallow seas, *Philos. Trans. R. Soc. A*, *221*, 239–264.

Kobayashi, M. H., J. M. C. Pereira, and J. C. F. Pereira (1999), A conservative finite-volume second-order-accurate projection method on hybrid unstructured grids, *J. Comput. Phys.*, *150*, 40–75, doi:10.1006/jcph.1998.6163.

Loder, J. W., and D. A. Greenberg (1986), Prediction positions of tidal fronts in the Gulf of Maine region, *Cont. Shelf Res.*, *6*, 397–414, doi:10.1016/0278-4343(86)90080-4.

Loder, J. W., J. A. Shore, C. G. Hannah, and B. D. Petrie (2001), Decadal-scale hydrographic and circulation variability in the Scotia-Maine region, *Deep Sea Res., Part II*, *48*, 3–35, doi:10.1016/S0967-0645(00)00080-1.

Lynch, D. R., and C. E. Naimie (1993), The M_2 tide and its residual on the outer bank of the Gulf of Maine, *J. Phys. Oceanogr.*, *23*, 2222–2253, doi:10.1175/1520-0485(1993)023<2222:TMTAIR>2.0.CO;2.

McLellan, H. (1958), Energy considerations in the Bay of Fundy system, *J. Fish. Res. Board Can.*, *15*(2), 115–134, doi:10.1139/f58-008.

Mellor, G. L., and T. Yamada (1982), Development of a turbulence closure model for geophysical fluid problem, *Rev. Geophys.*, *20*, 851–875, doi:10.1029/RG020i004p00851.

Moody, J. A., et al. (1984), Atlas of tidal elevation and current observations on the northeast American continental shelf and slope, *U.S. Geol. Surv. Bull.*, *1611*, 122 pp.

Mountain, D. G., and P. F. Jessen (1987), Bottom waters of the Gulf of Maine, *J. Mar. Res.*, *45*, 319–345, doi:10.1357/002224087788401160.

Roworth, E., and R. Signell (1998), Construction of digital bathymetry for the Gulf of Maine, *Open File Rep., 98-801*, U.S. Geol. Surv., Woods Hole, Mass. [Available at http://pubs.usgs.gov/of/1998/of98-801/]

Shearman, K., and S. J. Lentz (2004), Observations of tidal variability on the New England shelf, *J. Geophys. Res.*, *109*, C06010, doi:10.1029/2003JC001972.

Simpson, J. H., and J. R. Hunter (1974), Fronts in the Irish Sea, *Nature*, *250*, 404–406, doi:10.1038/250404a0.

Smagorinsky, J. (1963), General circulation experiments with the primitive equations, I. The basic experiment, *Mon. Weather Rev.*, *91*, 99–164, doi:10.1175/1520-0493(1963)091<0099:GCEWTP>2.3.CO;2.

Smith, P., R. W. Houghton, R. G. Fairbanks, and D. G. Mountain (2001), Interannual variability of boundary fluxes and water mass properties in the Gulf of Maine and on Georges Bank, *Deep Sea Res., Part II*, *48*, 37–70, doi:10.1016/S0967-0645(00)00081-3.

Werner, S. R., R. C. Beardsley, S. J. Lentz, D. L. Hebert, and N. S. Oakey (2003), Observations and modeling of the tidal bottom boundary layer on the southern flank of Georges Bank, *J. Geophys. Res.*, *108*(C11), 8005, doi:10.1029/2001JC001271.

Zhong, L., and M. Li (2006), Tidal energy fluxes and dissipation in the Chesapeake Bay, *Cont. Shelf Res.*, *26*, 752–770, doi:10.1016/j.csr.2006.02.006.

R. C. Beardsley and R. Limeburner, Department of Physical Oceanography, Woods Hole Oceanographic Institution, Woods Hole, MA 02543, USA. (rbeardsley@whoi.edu; rlimeburner@whoi.edu)

C. Chen, G. W. Cowles, H. Lin, J. Qi, Y. Sun, and Q. Xu, School for Marine Science and Technology, University of Massachusetts Dartmouth, New Bedford, MA 02744, USA. (c1chen@umassd.edu; gcowles@umassd.edu; qxu@umassd.edu)

H. Huang, Department of Oceanography and Coastal Sciences, School of the Coast and Environment, Louisiana State University, Baton Rouge, LA 70803, USA. (hhuang7@lsu.edu)